Applied Catalysis B: Environmental 336 (2023) 122894

Contents lists available at ScienceDirect

Applied Catalysis B: Environmental

journal homepage: www.elsevier.com/locate/apcatb

Effects of SO_2 poisoning and regeneration on spinel containing CH_4 oxidation catalysts

Natalia Diaz Montenegro, William S. Epling *

Department of Chemical Engineering, University of Virginia, United States

ARTICLE INFO

Keywords:
Methane oxidation
Sulfur poisoning
Catalyst regeneration
Oxygen storage capacity
Spinel catalyst

ABSTRACT

Methane oxidation under periodic conditions and the oxygen storage capacity of a bilayer $Pt/Pd/Al_2O_3$ over a $Mn_{0.5}Fe_{2.5}O_4$ spinel catalyst were studied before and after SO_2 exposure, and after simulated regeneration conditions. Prior to sulfur exposure, improvement in CH_4 oxidation conversion under periodic conditions compared to steady-state conditions was observed. After sulfur exposure at 100 °C, there was a loss in CH_4 oxidation performance and a loss of oxygen storage capacity of the spinel material. The extent of regeneration from sulfur poisoning depends on the ability to induce the decomposition of sulfate species, and while all regeneration methods tested in this study did improve CH_4 conversion, regeneration methods under periodic conditions induced greater sulfur species desorption from the catalyst surface leading to improved CH_4 conversion. Key regeneration parameters – temperature, feed composition, modulation amplitude and frequency – were optimized to induce S species decomposition and correlated to CH_4 oxidation activity recovery.

1. Introduction

Due to the abundance of natural gas in the United States [1] and relatively high fuel efficiency, natural gas engines are an attractive alternative to gasoline or diesel engines. In terms of emissions, they release less NO_x, CO and particulate matter into the atmosphere compared to diesel engines [2,3]. However, the main hydrocarbon found in natural gas is methane (CH_4), and since CH_4 is a powerful greenhouse gas [4], limiting CH_4 emissions from natural gas engine exhaust is necessary to lessen the effects of global warming and to comply with the 0.1 g/bhp-hr methane emission standard for heavy-duty vehicles and 0.05 g/mile for small pick-up trucks and vans set by the Environmental Protection Agency [5]. Current methane oxidation catalysts (MOCs), which operate at the stoichiometric air-to-fuel ratio, run into several challenges. First, due to the stable C-H bond (450 kJ/mol) and low sticking coefficient of CH_4 [6,7], high exhaust aftertreatment temperatures (T > 500 °C) and high precious metal loadings are needed to significantly reduce CH_4 emissions. Second, the mode of engine operation at the stoichiometric point provides a rather narrow window for the simultaneous conversion of CH_4, CO and NO_x. Third, the added sulfur-based odorant to natural gas can lead to a loss in MOC performance over time [3,8,9]. Based on these reasons and others, the development of new MOC formulations is needed to improve low temperature CH_4 oxidation activity.

$$CH_4 + 2O_2 \rightarrow CO_2(CO) + 2H_2O \quad (1)$$

$$CO \quad + 1/2O_2 \rightarrow CO_2 \quad (2)$$

$$CH_4 + 4NO \rightarrow 2N_2(N_2O, NH_3) + CO_2 + 2H_2O \quad (3)$$

Commercial MOCs are composed of a cordierite substrate in a honeycomb structure, on which a high surface area support, such as Al_2O_3 combined with a CeO_2-based oxygen storage material is washcoated. On this high surface area support, a combination of Pt group metal (Pt, Pd, or Rh) nanoparticles is deposited [3,9,10]. The precious metal materials are the active centers where MOC chemistry occurs (Eqs. (1)–(3)).

The CeO_2-based oxygen storage material is added to MOC formulations to alleviate the effects of changes in the air-to-fuel ratio during operation. In oxygen-deficient environments, CeO_2 reduces to CeO_{2-x}, and the released oxygen is used in the reactions described above (Eqs. (1)–(2)), which also creates oxygen vacancies at the surface. Once there is excess oxygen, oxygen vacancies are replenished with gas-phase O_2 leading to the re-oxidation of CeO_2 to maintain the air-to-fuel ratio at stoichiometric conditions (Eq. (4)) [11,12].

$$CeO_2 \leftrightarrow CeO_{2-x} + \frac{x}{2}O_2 \quad (4)$$

* Corresponding author.
E-mail address: wsepling@virginia.edu (W.S. Epling).

https://doi.org/10.1016/j.apcatb.2023.122894
Received 24 February 2023; Received in revised form 17 May 2023; Accepted 18 May 2023
Available online 19 May 2023

Current research trends prioritize improving precious metal utilization and new material discovery to promote MOC performance and tackle the challenges mentioned above. Due to their low cost, catalytic tunability and high abundance, spinel materials have been explored as candidates for diesel aftertreatment technologies, especially for hydrocarbon, soot and NO_x removal [13–23]. Spinel oxides have an AB_2O_4 crystal structure, where A^{2+} transition metal ions occupy tetrahedral sites, while B^{3+} ions occupy octahedral sites in the lattice. As potential oxygen storage materials, spinel materials show promise as the lattice oxygen in the framework can be used without any structural impact. For example, Cu-Mn spinel materials have more readily available oxygen during transient conditions compared to commercial CeO_2-based oxygen storage materials [24,25]. Plus, the addition of these spinel-based oxygen storage materials could also reduce the amount of PGM added to MOC formulations [26–28].

Due to their difficulty in being oxidized, one way to improve low temperature conversion of saturated hydrocarbons, such as methane [29–32] and propane [33], is by periodically changing the oxygen concentration in the feed composition. For Pt-based catalysts, the improvement in low temperature CH_4 conversion under periodic conditions is due to the formation of a partially oxidized Pt surface that favors methane dissociation at lower temperatures. Plus, periodic conditions mitigate the oxygen poisoning effect on Pt active sites [34–36]. Previous studies have reported that under periodic operation, the temperature at which 50% CH_4 conversion is achieved under a simulated exhaust feed over a dual-layer MOC formulation that includes a PGM layer (Pt:Pd 19:1, 30 g/ft^3) and a $Mn_{0.5}Fe_{2.5}O_4$ spinel layer (25 wt% $Mn_{0.5}Fe_{2.5}O_4/Al_2O_3$, 100 g/L) decreased by ~85 °C compared to steady-state inlet conditions [28]. The addition of the $Mn_{0.5}Fe_{2.5}O_4$ spinel as an oxygen storage material provided extra oxygen during the oxygen-deficient phases during periodic conditions, which maintained the oxygen balance closer to the stoichiometric point and curbed the production of undesirable byproducts, such as NH_3 [28]. The catalyst structure of this MOC formulation can also be designed to maximize the storage/release capabilities of $Mn_{0.5}Fe_{2.5}O_4$ layer under periodic conditions [37] and minimize potential inhibitory effects that may occur at high temperatures, such as species migration and active Pt site blockage [37,38]. Periodic operation can also be optimized by finding an optimal amplitude and frequency to promote CH_4 oxidation activity [38–40].

Natural gas exhaust contains ppm levels of SO_2 due to the combustion of the odorant added to the fuel. Over time, these low levels of SO_2 may have a detrimental effect on catalyst performance and structure, but the extent of deactivation depends on the precious metal and support used [9,41–44]. In the case of Pd-based catalysts, SO_2 can strongly chemisorb to Pd sites and form inactive $PdSO_4$ species [43,45,46]. Unlike Pd, Pt sites do not form $PtSO_4$ species, but weakly adsorbed S species, such as sulfides and molecular SO_2, can form or adsorb [47]. Regarding the support, sulfating supports, such as Al_2O_3 and CeO_2, interact with SO_2 to form sulfate species (SO_4^{-2}) allowing precious metal sites to remain available until the support is saturated. On the other hand, non-sulfating supports, such as SiO_2, are not able to form sulfate species, leaving precious metals the only site where SO_2 can chemisorb [42,48–52]. Additionally, reaction conditions, especially the presence of oxygen and adsorption temperature, and precious metal nanoparticle size affect the formation of more oxidized S species, such as sulfite (SO_3^{-2}) and sulfate (SO_4^{-2}) species [47,52–54]. Ultimately, the presence of S-related species leads to the loss of CH_4 oxidation performance due to inhibition of active sites and chemistry at the metal-support interface, especially for CeO_2-based supports. However, the addition of small amounts of Pt to Pd-based methane oxidation catalysts does offer some sulfur resistance [53–57]. There is ample literature regarding PGM-based aftertreatment catalyst materials and the impact of S on them; however, since transition metal oxides have become an alternative to PGM-based aftertreatment systems, their sulfur resistance must also be assessed for implementation. For example, Mn-based catalysts can easily form $MnSO_4$ species which leads to the loss of active sites, especially for NO oxidation [58,59].

To recover performance, the effects of SO_2 poisoning can be reversed via a catalyst regeneration strategy. Common regeneration techniques usually involve high temperature treatments to induce the decomposition of the adsorbed S species from the catalyst surface [53,54,56,57,60–73]. For example, with Pt/Pd-based catalysts supported on Al_2O_3, molecular SO_2 and surface SO_3^{-2} species decompose and desorb around 400 °C from the catalyst surface, while more stable S species, such as SO_4^{-2}, do not decompose until temperatures higher than 600 °C [53]. Regarding the regeneration of Pd active sites, the regeneration environment influences the final Pd state after $PdSO_4$ decomposition, which affects methane oxidation activity recovery [64,74]. One way to lower the temperature of the decomposition of the adsorbed S species from the catalyst surface is by altering the regeneration environment. For example, reducing environments with H_2 at 600 °C were found to remove all SO_4^{-2} species which led to the full recovery of CH_4 oxidation performance for Pd-based catalysts [67]. Other studies have shown sulfate decomposition at high temperature could also be induced by alternating the feed composition between the presence of a reductant (i.e., CH_4) and the presence of oxygen [61,62,64,68,69].

While the addition of a $Mn_{0.5}Fe_{2.5}O_4$ spinel layer to bimetallic Pt-Pd catalysts has been studied in terms of CH_4 oxidation, steam reforming, and under periodic conditions [28,37,38,75,76], the effects of SO_2 on this MOC formulation have yet to be explored, which is imperative for aftertreatment implementation. Here, we have studied the effects of SO_2 and model catalyst regeneration protocols on CH_4 oxidation performance and oxygen storage capacity of a bilayer PGM + $Mn_{0.5}Fe_{2.5}O_4$ spinel catalyst under steady-state and inlet feed modulated conditions. We focused on the response to SO_2 of the $Mn_{0.5}Fe_{2.5}O_4$ spinel material as an oxygen storage material, and its impact on CH_4 oxidation performance. Different regeneration methods were applied and evaluated in terms of CH_4 oxidation activity recovery and S release, measured as SO_2, from the sample. Then, temperature, feed composition and modulation parameters, such as amplitude and frequency, were evaluated during regeneration for their impact on inducing the decomposition of S species on the catalyst, to improve CH_4 oxidation performance.

2. Experimental methods

2.1. Catalyst information and experimental set-up

All powder and monolith samples were provided by CDTi Advanced Materials, Inc, and a summary of their compositions and configurations is displayed in Fig. 1 and in Table S1. The PGM only monolith sample is a single-layer catalyst that is wash-coated onto a cordierite monolith substrate. The catalyst is composed of Pt/Pd deposited onto Al_2O_3. The Pt:Pd loading is 30 g/ft^3 of monolith, with a Pt:Pd mass ratio of 19:1. The PGM + spinel monolith sample is a dual layer catalyst that includes a top layer of the same Pt/Pd catalyst, and a bottom layer of $Mn_{0.5}Fe_{2.5}O_4$ spinel material. The spinel layer loading is 2832 g/ft^3 with 25 wt% spinel material supported on Al_2O_3. Both layers were wash-coated, sequentially, onto a cordierite monolith. For experiments with the monolith samples, the gas hourly space velocity (GHSV) was 60,000 hr^{-1} with a total flowrate of 1 L/min. Monolith samples were 6 mm in diameter and 28 mm in length. The $Mn_{0.5}Fe_{2.5}O_4$ spinel powder (referred to as Mn-Fe spinel powder) includes the spinel material with the same composition as the spinel layer of the monolith sample, i.e. 25% spinel on Al_2O_3. For the powder sample experiments, 15 mg of spinel powder was diluted with 150 mg of cordierite, and a total flowrate of 300 sccm was used. Prior to all experiments, all catalysts were pretreated in 10% O_2 in N_2 at 550 °C for 45 min. Surface area and precious metal dispersion have been reported in previous studies [37].

Each catalyst sample was placed in a quartz tube inside a Thermo Scientific Lindberg/Blue tube furnace as part of a flow reactor system. Bronkhorst and MKS mass flow controllers were used to adjust inlet gas flowrates. Type K thermocouples at the catalyst inlet and outlet were

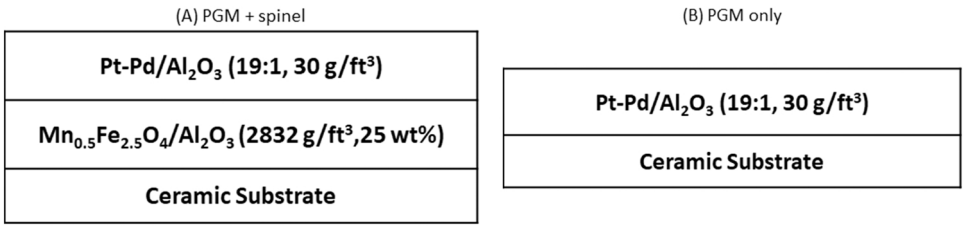

Fig. 1. – Compositions and configuration for the monolith samples: (A) PGM + spinel and (B) PGM only.

used to monitor the temperature, and the inlet temperature was used to plot results. For all experiments, outlet CH_4, CO, CO_2, H_2O, SO_2, SO_3 and COS gas concentrations were measured using an MKS MultiGas 2030 FTIR Spectrometer gas analyzer. Data were acquired at a rate of 1 Hz. To provide the gas mixtures, specialty gas cylinders were purchased from Praxair Inc and N_2 was generated using an On Site Gas System N-20 nitrogen generator. Water vapor was introduced using a Bronkhorst CEM system. To avoid sulfur deposition along the reactor lines, stainless steel reactor lines treated with a sulfinert coating were purchased from Swagelok. Reactor lines were heated to temperatures above 100 °C to avoid water condensation.

2.2. CH_4 oxidation activity and oxygen consumption measurements

The CH_4 oxidation activity assessment was performed using a temperature programmed reaction protocol with a temperature ramp of 5 °C/min. For periodic operation experiments, an inlet gas composition of 1500 ppm CH_4, with varying O_2 amounts in a N_2 balance was used. For the preliminary experiments in Fig. 2, the oxygen concentration of the inlet gas was varied from 3000 ppm to 1%. For these experiments, a four-way solenoid air control valve purchased from Grainger (part #6JJ44) was used to switch between O_2/N_2 flow and N_2. For steady-state experiments, the inlet oxygen concentration was 2750 ppm. Note, water was not included in the bulk of the experiments. Although water is ubiquitous in combustion exhaust gas, we intentionally excluded it to keep things simpler as we begin to understand this relatively new catalytic system.

As a measure of the available reactive oxygen on the Mn-Fe spinel material, the amount of O consumed during a 2-minute CO pulse – $O_{consumed}$ – was calculated between 200 and 600 °C in increments of 100 °C. After the O_2 pretreatment at 500 °C, the reactor was cooled to 200 °C in the presence of 10% O_2 in N_2. Once the temperature stabilized, oxygen was turned off and a N_2 purge was introduced for 15 min. Using the four-way switching valve, a pulse of 0.8% CO in N_2 was introduced for 2 min, and the concentration of CO_2 was monitored. After 5 min, 10% O_2 in N_2 flow was reintroduced to the reactor to reoxidize the sample, and the temperature was increased. Assuming that the oxygen that leads to the production of CO_2 comes exclusively from the Mn-Fe spinel material, $O_{consumed}$ was calculated using Eq. (5) using the CO_2 produced during the 2-minute CO pulse divided by the mass of the catalyst, $m_{Mn\text{-}Fe\ spinel}$. This measurement provides a way to evaluate changes in the available O in the spinel as a function of temperature, S exposure and regeneration conditions.

$$O_{consumed} = \frac{\int_0^t [CO_2]dt}{m_{Mn-Fe \quad Spinel}} \tag{5}$$

Periodic operation conditions used less than 2-minute cycles, this $O_{consumed}$ value was simply used to probe the changes in the available oxygen of the Mn-Fe spinel material.

2.3. Sulfur poisoning

To assess the effects of SO_2 exposure on the CH_4 oxidation activity and the amount of available O in the 2-minute CO pulse, $O_{consumed}$, the samples were exposed to 10 ppm of SO_2 in a N_2 balance at 100 °C after the 550 °C pretreatment described above. Once the SO_2 outlet concentration recorded by the FTIR reached the inlet 10 ppm concentration, a N_2 purge was introduced to clear the lines and remove weakly absorbed sulfur species from the sample. Then, the CH_4 oxidation temperature programmed reaction activity test, as described above, was again performed. For the oxygen consumption measurements, after SO_2 exposure at 100 °C, SO_2 was turned on during the reoxidation steps between each temperature and turned off during the N_2 purge and CO pulse duration.

2.4. Catalyst regeneration

Different regeneration methods were applied and evaluated in the recovery of CH_4 oxidation activity and the amount of available O in the 2-minute CO pulse, $O_{consumed}$. After SO_2 exposure at 100 °C, each sample was either exposed to 10% O_2, 3% H_2 or 0.8% CO in N_2 and a 10 °C/min temperature ramp to 600 °C, followed by an isothermal hold at 600 °C for 45 min. After each regeneration treatment, the sample was pretreated in 10% O_2 in N_2 balance at 550 °C for 45 min. Then, the reactor was cooled down to 100 °C in the presence of 10% O_2 in N_2 balance, and

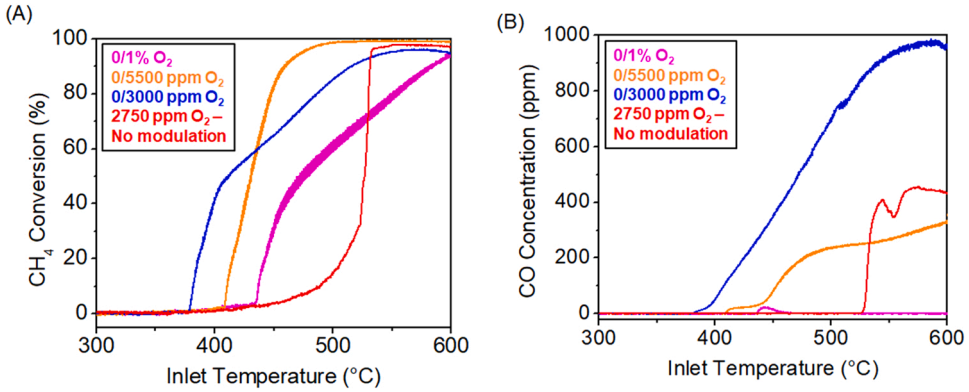

Fig. 2. (A) CH_4 conversion and (B) CO formation using the PGM + spinel sample under no modulation and with periodic conditions during the CH_4 temperature programmed reaction ([CH_4] = 1500 ppm, [O_2] = varied, frequency = 0.25 Hz).

the CH_4 oxidation and oxygen consumption activity tests were performed.

Separately, higher temperature regeneration methods were also used. Table 1 summarizes the regeneration conditions the catalyst sample experienced for 45 min at 700 °C after SO_2 exposure at 100 °C. For these regeneration treatments, the regeneration protocol is described by Schematic S1. After the CH_4 oxidation temperature programmed reaction, the temperature was held at 600 °C for 60 min. Then, the temperature was increased at 10 °C/min to 700 °C under regeneration conditions described in Table 1, and the temperature was held for 45 min at 700 °C. The temperature was then lowered to 600 °C in CH_4 oxidation conditions.

3. Results and discussion

3.1. Role of $Mn_{0.5}Fe_{2.5}O_4$ addition on CH_4 oxidation during periodic conditions

First, we investigated the effects of periodic conditions on methane oxidation activity using the PGM + spinel sample. Such periodic conditions not only mimic realistic operation conditions more closely due to changes in the air-to-fuel ratio (AFR) during the driving cycle, but also the varying oxygen concentration over the catalyst surface improves catalytic performance [77]. Fig. 2A shows the methane conversion on the PGM + spinel sample with no modulation and with periodic conditions. Under periodic conditions, the onset temperature for methane conversion increases with increased oxygen concentration in the oxygen containing phase. The methane oxidation onset temperature was highest under no modulation conditions. This is also consistent with prior literature, where when including H_2O in the mixture the same improvement with modulation was noted [28]. The initial increase in conversion as a function of temperature is also faster with modulation. The onset temperature increasing with increasing oxygen suggests that the formation of the more active partially oxidized Pt surface that occurs during periodic conditions depends on the oxygen concentration of the inlet gas, as might be expected. The formation of CO during periodic and no modulation conditions is shown on Fig. 2B. The presence of byproduct CO indicates that partial oxidation (Eq. (6)) and/or steam reforming (Eq. (7)) of CH_4 occurred. For the lowest O_2 concentration under modulation conditions, 3000 ppm, as temperature increased past 400 °C, the rate of change in CH_4 conversion as a function of temperature slows due to the lack of oxygen availability, which also leads to the greater formation of CO. In the case of the highest O_2 concentration in the O_2-containing phase, 1%, the more abundant oxygen may lead to oxygen poisoning of Pt sites at high temperatures which slows CH_4 conversion [30,34–36,78]. As oxygen becomes more abundant, the formation of CO decreases as expected. With the intermediate 5500 ppm O_2 concentration, full conversion of CH_4 was achieved in the temperature range used. With no modulation conditions and the 3000 ppm oxygen, complete or near complete conversion of CH_4 was also achieved suggesting that enough O was available to oxidize CH_4 without poisoning the Pt sites; however, the onset of CH_4 oxidation occurs at higher temperatures compared to those that included modulation. Since the oxygen concentration is slightly lower than the stoichiometric point, under no modulation conditions, some CO formation is observed as well. The improved CH_4 conversion under periodic conditions on the PGM + spinel monolith sample has also been observed in previous studies [28,37]. Furthermore, this improvement in CH_4 conversion under periodic conditions is observed under simple ($CH_4 + O_2 + N_2$) inlet gas conditions, such as those used to obtain the results in Fig. 2, as well as more complex simulated exhaust feeds, such as one containing CH_4, O_2, H_2O, CO, H_2, NO and CO_2, as shown in Fig. S1.

$$CH_4 + \frac{1}{2}O_2 \leftrightarrow 2H_2 + CO \quad (6)$$

$$CH_4 + H_2O \leftrightarrow 3H_2 + CO \quad (7)$$

To corroborate that the addition of an oxygen storage material would improve catalytic performance of a PGM-based sample [28,37,79], we performed 2-minute cycles, with one phase containing O_2 and the other none ($[O_2] = 0$ or 5500 ppm) on both the PGM + spinel and PGM only samples. Methane conversions using this protocol at 315, 345 and 370 °C are shown in Fig. 3, where the phases containing no oxygen have been shaded. For the PGM + spinel monolith sample, a sharp increase in CH_4 conversion is seen with the switch to the oxygen-deficient gas environment for all temperatures, and then the conversion eventually decreases with time. Once the feed switches to the oxygen-containing environment, only a slight increase in methane conversion is observed and quickly decreases. In the following oxygen-absent phase, the high CH_4 conversion peak is again observed. In the case of the PGM only sample, only a small peak in CH_4 conversion is observed during the switch to the oxygen absent phases, and no conversion is observed during the oxygen-containing phases. The 2-minute cycle results show that the incorporation of the Mn-Fe spinel layer with the PGM leads to an increase in CH_4 conversion during the oxygen-deficient phases compared to the PGM only sample. This has been attributed to the ability of the Mn-Fe spinel layer to store and release oxygen depending on the operating conditions, while maintaining precious metal sites in a more favorable oxidation state for CH_4 oxidation [28,37]. As oxygen is released from the spinel lattice to the PGM sites during the oxygen-deficient phases, oxygen vacancies are created. Once oxygen is reintroduced into the feed, gas-phase oxygen dissociates, and the oxygen vacancies created in the spinel lattice are refilled. The 2-minute pulse experiment results suggest that oxygen from the Mn-Fe spinel layer is released during the oxygen-deficient phases and participates in the conversion of CH_4. However, this oxygen reservoir depletes over time leading to the CH_4 conversion decrease with time during this phase. In the oxygen-containing phase, the oxygen reservoir is replenished since in the next oxygen-deficient phase, the CH_4 conversion peak is of the same magnitude as the previous one. However, during the oxygen-containing phase, a small CH_4 conversion peak for all temperatures is observed due to the newly introduced oxygen; however, CH_4 conversion quickly ceases since the oxygen concentration during this phase leads to oxygen poisoning of the precious metal sites. Direct comparison of the CH_4 conversion under the CH_4 temperature programmed oxidation of these two catalysts can also be found in Fig. S2.

As a measure of O accessibility during the oxygen-deficient phases, the amount of oxygen consumed during a 2-minute CO pulse ($O_{consumed}$) for the Mn-Fe spinel material was calculated. Fig. 4 shows these amounts from 200 to 600 °C. As temperature increases, the calculated $O_{consumed}$ from the Mn-Fe spinel material increases showing that more oxygen can be accessed during periodic conditions with increasing temperature. In the presence of a reductant, for example CO, Mn and Fe cations in the spinel lattice can reduce to their metallic forms (shown in Eqs. (8) and (9)), which would release lattice oxygen. This is what leads to the production of CO_2 during the CO pulse. Different extents of reduction, or different relative amounts of spinel being reduced, occur at each temperature. To rule out thermal decomposition of the Mn-Fe spinel as a possible oxygen source, a temperature programmed desorption (TPD) study showed that under inert flow conditions, although desorbed oxygen was observed at high temperatures, the total amount of oxygen released corresponds to only a small fraction (~0.1%) of the total oxygen storage capacity of the Mn-Fe spinel material [37]. Therefore, the

Table 1
Regeneration operating conditions.

#	O_2 (%)	H_2 (%)	CH_4 (ppm)	Cycling Frequency (Hz)
1	-	3%	-	N/A
2	0/0.55%	-	1500	0.25
3	0/0.55%	-	1500	0.0625
4	0/0.55%	0.1%	1500	0.0625

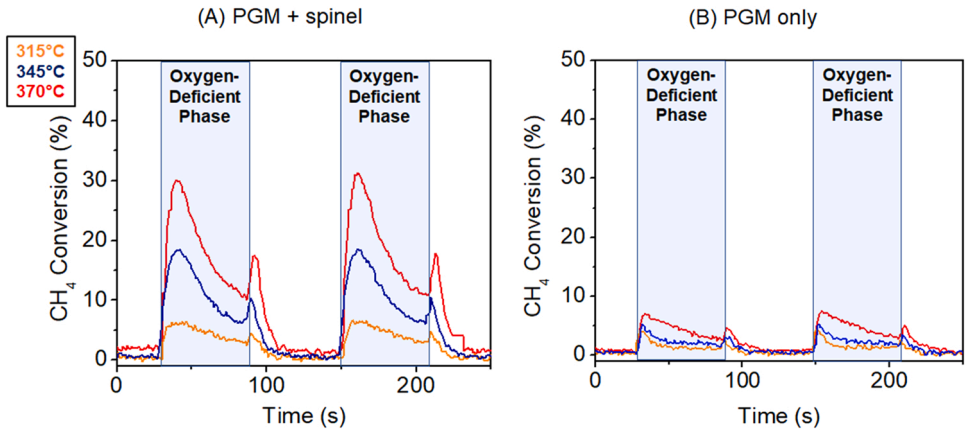

Fig. 3. CH_4 conversion using 2-minute cycles ([CH_4] – 1500 ppm, [O_2] – 0/5500 ppm, N_2 balance) on (A) PGM + spinel and (B) PGM only samples as a function of time. Oxygen-deficient phases are shaded in blue.

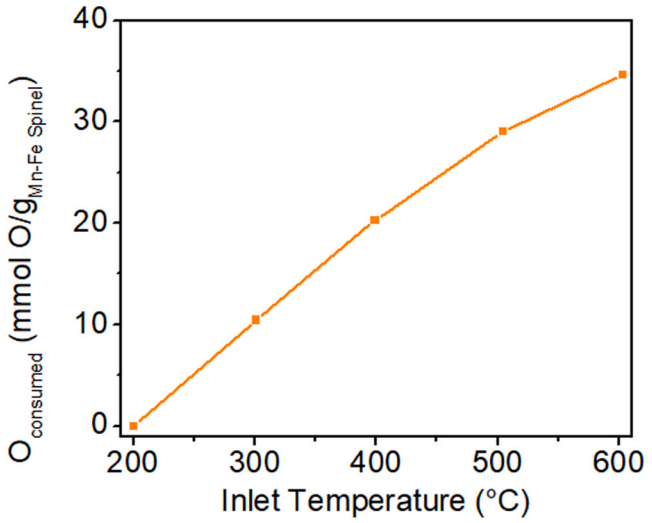

Fig. 4. Calculated $O_{consumed}$ of the fresh Mn-Fe spinel powder sample as a function of temperature. $O_{consumed}$ was calculated by the production of CO_2 during 0.8% CO/N_2 pulse for two minutes in the absence of oxygen.

oxygen that leads to the production of CO_2 during this CO protocol comes exclusively from the lattice oxygen released during the reduction of the Mn-Fe spinel material.

$$Mn_{0.5}Fe_{2.5}O_4 + CO \rightarrow 0.5MnO + 2.5FeO + CO_2 \quad (8)$$

$$Mn_{0.5}Fe_{2.5}O_4 + 3.5CO \rightarrow 0.5MnO + 2.5Fe + CO_2 \quad (9)$$

3.2. Sulfur impact on CH_4 oxidation activity and $O_{consumed}$

After SO_2 exposure at 100 °C, the CH_4 oxidation temperature programmed reaction under periodic conditions ([O_2] – 0/5500 ppm, [CH_4] – 1500 ppm, frequency – 0.25 Hz) was performed using the PGM + spinel sample. The CH_4 conversion for the fresh and SO_2-exposed samples, and the SO_2 concentration profile, representing the amount of SO_2 desorbed, during the temperature ramp are shown in Fig. 5A. Sulfur exposure at 100 °C leads to both promoting and inhibiting effects on CH_4 oxidation. Between 370 and 400 °C, the CH_4 conversion is higher after SO_2 exposure, whereas at higher temperature the conversion is lower. An increase in low-temperature hydrocarbon conversion (specifically for propane [80–82] and methane [83]) has been previously reported on S-exposed Pt/Al_2O_3 catalysts. In the case of propane oxidation, the formation of new active sites at the metal-support interface promotes hydrocarbon dissociation. We speculate the same might occur here.

During the temperature ramp, two SO_2 desorption peaks were observed. No SO_3, COS or H_2SO_4 was detected. Based on the literature, the low temperature desorption peak (located at 150 °C) corresponds to the desorption of SO_2 from physisorbed SO_2 and decomposed sulfite (SO_3^{-2}) species on the catalyst surface, while the higher temperature desorption peak, located at temperatures above 500 °C, corresponds to the desorption of SO_2 from the decomposition of sulfate species [42, 49–52].

The temperature program was extended to include an isothermal hold at 600 °C to further look into the evolution of the higher

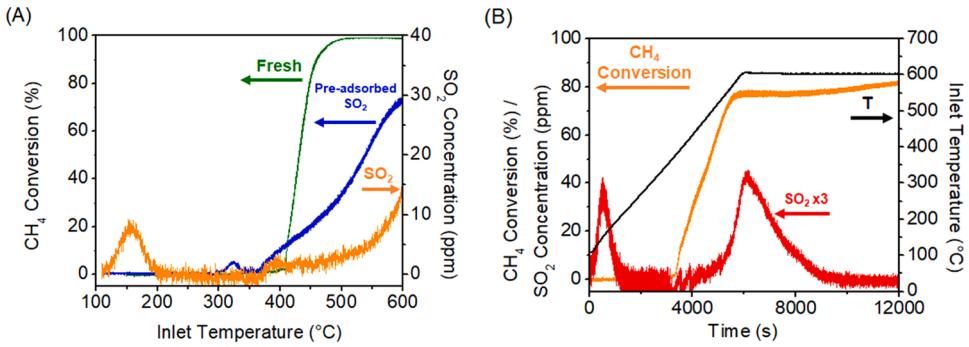

Fig. 5. (A) CH_4 conversion before and after SO_2 exposure at 100 °C under periodic conditions and the SO_2 concentration during the CH_4 temperature programmed reaction ([CH_4] – 1500 ppm, [O_2] – 0/5500 ppm, frequency – 0.25 Hz), (B) CH_4 conversion and SO_2 profile after SO_2 exposure at 100 °C during the same experiment as shown in panel A, but also including the isothermal hold at 600 °C for 1 h.

temperature SO_2 desorption peak. Methane conversion on the PGM + spinel sample and the SO_2 profile during the latter part of the temperature ramp and the isothermal hold at 600 °C are shown in Fig. 5B. During the isothermal hold at 600 °C, CH_4 conversion initially stayed constant at ~75%; however, after 30 min, CH_4 conversion began to slowly increase and continued to until the end of the isothermal hold. During the isothermal hold, the release of SO_2 was observed, and while SO_2 was observed, CH_4 conversion remained constant. Once SO_2 release ended, CH_4 conversion began to increase. During the initial part of the isothermal hold, the sulfate species were decomposing, likely those close to the active precious metal sites, or began migrating to the precious metal sites to decompose [84]. Ultimately, the decomposition of S species continues to influence precious metal sites in terms of CH_4 oxidation, and once those in proximity to the active sites are removed or the migration of S species toward the precious metal sites ceases, CH_4 conversion increases.

To assess the effects of SO_2 on the calculated $O_{consumed}$ of the Mn-Fe spinel layer during the 2-minute CO pulse, the amount of CO_2 formed during the CO pulse experiment was again calculated using just the Mn-Fe spinel powder. Fig. 6A shows the comparison of the fresh and SO_2-exposed $O_{consumed}$ of the Mn-Fe spinel powder. In the presence of SO_2, little to no $O_{consumed}$ was observed in the 200–500 °C temperature range, suggesting that SO_2 poisons the reactive O sites on the Mn-Fe spinel powder. In terms of CH_4 oxidation under periodic conditions, no oxygen from the Mn-Fe spinel material would be provided which could also contribute to the shift in CH_4 conversion to higher temperatures observed in Fig. 5A. No SO_2 desorption from the spinel occurred in this temperature range. However, $O_{consumed}$ was observed at 600 °C. At these high temperatures, as CO was introduced to the reactor, the appearance of both CO_2 and SO_2 was observed as shown in Fig. 6B. CO reduces the sulfate species leading to the release of S from the catalyst surface. Once the CO pulse ends, SO_2 desorption ends.

3.3. Catalyst regeneration methods

Common literature regeneration methods, such as oxidizing and reducing environments, as well as oscillating between them, were used to assess their effectiveness in the decomposition of the adsorbed S species from the catalyst surface. This should lead to increased $O_{consumed}$ of the Mn-Fe spinel material, and based on the results shown above, should lead to an increase in CH_4 conversion. The recovery of the $O_{consumed}$ during the 2-minute CO pulse of the Mn-Fe spinel material was first assessed, and the best regeneration method was then used to verify if CH_4 oxidation activity was recovered over the PGM + spinel sample. Fig. 7A shows the comparison of the $O_{consumed}$ of the fresh, SO_2-exposed, and regenerated Mn-Fe spinel powder after three different regeneration methods. A regeneration temperature of 600 °C was chosen based results shown in Figs. 5B and 6B, as well as literature results that show that this temperature can induce the decomposition of S species, especially sulfate (SO_4^{-2}) species [67]. All regeneration methods successfully recovered some $O_{consumed}$ for the Mn-Fe spinel powder, with the extent of recovery a function of the gas composition during the regeneration treatment. Fig. 7B shows the SO_2 profiles during the regeneration temperature ramp before the isothermal hold at 600 °C for 45 min. The SO_2 desorption profiles under reducing environments are far larger compared to the SO_2 desorption profile during oxidative conditions, consistent with prior results [52,62,66]. A sulfur mass balance during the adsorption and regeneration phase for these three regeneration treatments can be found in Table 2. Reducing environments induce more decomposition of the sulfate species (% desorbed > 30%), compared to the treatment in O_2 (% desorbed ≈ 2%).

Sulfates are readily formed on Al_2O_3 and CeO_2 with exposure to SO_2 [50]. Such sulfate species, on Pd/CeO_2 at least, decompose at lower temperatures in a reducing environment relative to an oxidizing environment [63,85] consistent with our observations. This is due to the reductant exposure leading to sulfate reduction and then S species desorption, whereas under oxidizing conditions, the sulfates remain stable to higher temperatures. Interestingly, reducing environments in both H_2 and CO at 600 °C led to an increased measure of $O_{consumed}$ at 600 °C compared to the fresh sample. In the literature, it has been hypothesized that oxygen from the decomposition of SO_4^{-2} species in CeO_2-based materials may contribute to the oxygen storage capacity process [85]. At 600 °C, as shown in Figs. 6B and S3, the CO pulse at 600 °C not only leads to CO_2 formation via consumption of oxygen from the spinel lattice, but also the desorption of SO_2 from the decomposition of sulfate species, which could lead to the increased $O_{consumed}$ compared to the fresh sample. Note, since the S mass balance did not close for all regeneration treatments, there is likely remaining S on the catalyst surface, and it still could impact catalytic activity.

Based on the recovery of $O_{consumed}$, reducing treatments can effectively regenerate the ability for the Mn-Fe spinel material to provide lattice oxygen by inducing the decomposition of S species from the catalyst surface. Reducing treatments were therefore applied to the PGM + spinel sample to assess if CH_4 oxidation activity was recovered. Fig. 8 shows the CH_4 conversion obtained using the fresh, SO_2-exposed, and H_2-regenerated at 600 °C samples, and the SO_2 concentration profile during the temperature ramp after the H_2 regeneration at 600 °C. At low temperatures (< 450 °C), the H_2 regeneration at 600 °C successfully recovered all CH_4 oxidation activity since CH_4 conversion profiles matched that for the experiment using the fresh sample. However, at higher temperatures, the rate of change in CH_4 conversion as a function of temperature slowed and ultimately only achieved ~77%. In evaluating the SO_2 desorption profile during the CH_4 oxidation temperature ramp, as CH_4 conversion achieves its maximum, SO_2 desorption is observed before the end of the temperature ramp. The sulfur mass balances during adsorption and desorption during the regeneration and

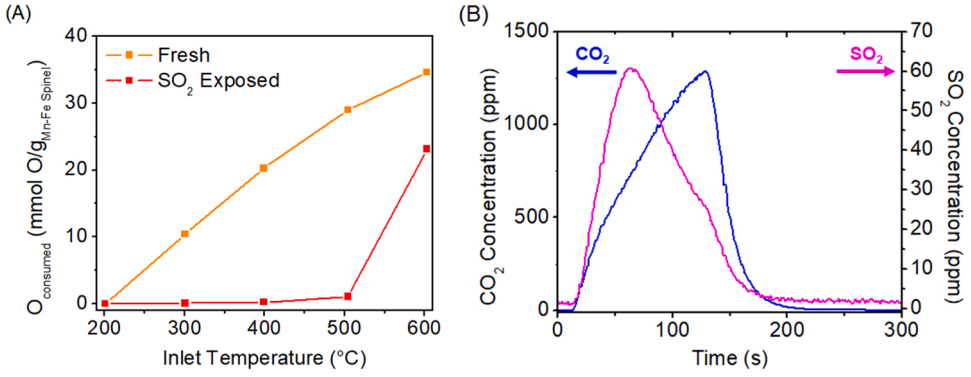

Fig. 6. (A) Comparison of the calculated $O_{consumed}$ of the fresh and SO_2-exposed Spinel Powder sample; (B) CO_2 and SO_2 profile during the CO pulse at 600 °C from the SO_2-exposed Spinel Powder sample. $O_{consumed}$ was calculated by the production of CO_2 during 0.8%CO/N_2 pulse for two minutes in the absence of oxygen.

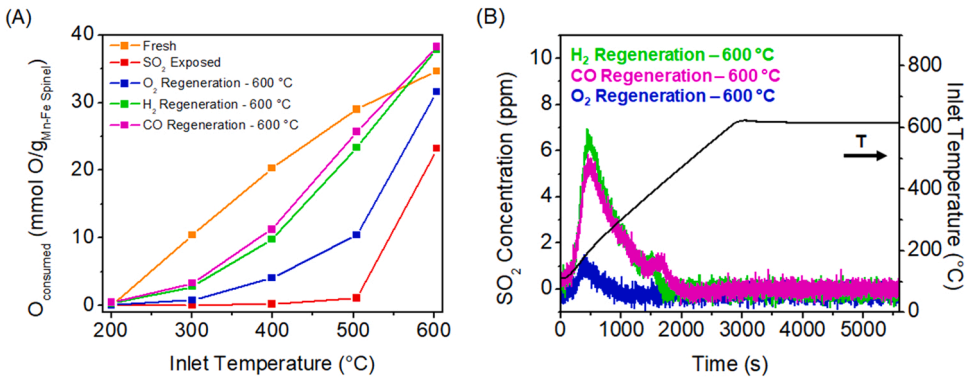

Fig. 7. (A) Comparison of $O_{consumed}$ for the fresh, SO_2 exposed and regenerated Spinel Only powder; (B) SO_2 profile during the regeneration ramps. After SO_2 exposure at 100 °C, each sample was either regenerated in 10% O_2, 3% H_2 or 0.8% CO in N_2 with a 10 °C/min temperature ramp to 600 °C, followed by an isothermal hold at 600 °C for 45 min. $O_{consumed}$ was calculated by the production of CO_2 during 0.8%CO/N_2 pulse for two minutes in the absence of oxygen.

Table 2 –
S mass balance after regeneration of the Mn-Fe spinel powder samples.

Regeneration Temperature (°C)	Regeneration Conditions	SO_2 Adsorbed (μmol)	SO_2 Desorbed (μmol)	% Desorbed
600	10% O_2 + N_2	3.0	0.1	2.3
600	3% H_2 + N_2	2.7	0.9	32
600	0.8% CO + N_2	2.6	0.9	35

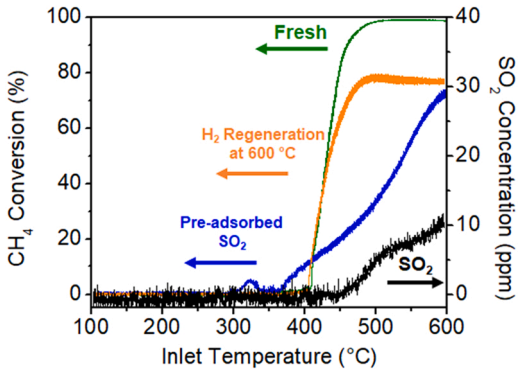

Fig. 8. Comparison of the CH_4 conversion using fresh, SO_2 exposed and H_2 regenerated PGM + spinel monolith samples, and the SO_2 profile during the CH_4 oxidation temperature reaction ramp after H_2 regeneration. After SO_2 exposure at 100 °C, each sample was exposed to 3% H_2 in N_2 and then subjected to a 10 °C/min temperature ramp to 600 °C, followed by an isothermal hold at 600 °C for 45 min. After the regeneration treatment, the sample was exposed to 10% O_2 in N_2 balance at 550 °C. Then, the reactor was cooled down to 100 °C in the presence of 10% O_2 in N_2 balance, and the CH_4 oxidation temperature program was performed.

CH_4 oxidation ramps can be found in Table 3.

Regarding the SO_2 desorption during the regeneration and CH_4 oxidation ramp, only 56% of the total SO_2 adsorbed was desorbed, suggesting that a fraction of S was decomposed under the regeneration and CH_4 oxidation steps, and the remaining S influences CH_4 oxidation performance. Since no low temperature desorbing S species were observed during the CH_4 oxidation temperature ramp, H_2 regeneration at 600 °C can decompose these species and recover $O_{consumed}$ from the Mn-Fe spinel material but falls short at inducing the decomposition of some other S species. Inhibition by SO_4^{-2} species is most likely impacting CH_4 oxidation performance, likely due to their stability and possibly also proximity to the active sites [66,82,86]. Furthermore, the pattern observed matches that in Fig. 5B, where CH_4 conversion plateaued and only began increasing once SO_2 desorption stopped. Another concern with high temperature regeneration treatments is the potential of irreversible deactivation via precious metal particle sintering or changes in oxygen storage. However, exposing the PGM + spinel sample to these H_2 regeneration conditions, but with no SO_2 exposure at 100 °C, led to no differences in the CH_4 oxidation performance, as shown in Fig. S4. Therefore, the unconventional CH_4 oxidation behavior at high temperatures is due to inhibition by residual SO_4^{-2} species, not caused by deactivation via sintering or changes in oxygen storage properties.

The effectiveness of the regeneration method at inducing the decomposition of S species depends on the gas composition as shown from the results above. However, those regeneration methods were not completely effective in the decomposition of stable SO_4^{-2} species, which have been noted to affect CH_4 oxidation activity at high temperatures [86]. Since the 600 °C regeneration technique induced the decomposition of some S species on the catalyst, increasing the regeneration temperature should lead to more S species decomposition. In the case of O_2 regeneration (Fig. S5A), two higher regeneration temperatures were tested, 650 and 700 °C, using the protocol described in Schematic S1. After each regeneration step, CH_4 conversion improved and ultimately reached 85%. Interestingly, in evaluating the SO_2 profile during the regeneration protocol (Fig. S5B), some SO_2 desorption occurred once CH_4 oxidation conditions were reintroduced after the O_2 regeneration steps. During the O_2 regeneration steps, the SO_4^{-2} species did not decompose. With the switch to CH_4 oxidation conditions, even though oxygen was present, exposure to CH_4 as a reductant led to the decomposition of SO_4^{-2} species as desorbed SO_2. This is consistent with studies that have shown improvement in CH_4 conversion under regeneration methods where the feed composition alternates between periods of high

Table 3
S mass balance after regeneration for the PGM + spinel monolith samples.

Regeneration Temperature (°C)	Regeneration Conditions	SO_2 Adsorbed (μmol)	SO_2 Desorbed During Regeneration Ramp (μmol)	SO_2 Desorbed During CH_4 Oxidation Ramp (μmol)	% Desorbed
600	3% H_2 + N_2	38.1	14.2	7.3	56%
700	CH_4 + H_2 + cycled [O_2] – 0/5500 ppm at 0.0625 Hz	42	-	36	87%

oxygen concentrations and the presence of reductant (i.e., CH_4) [57,61,62]. In the case of H_2 regeneration (Fig. S6A), regeneration temperatures at 650 and 700 °C were also tested. Methane conversion also improved after each regeneration step, again reaching 85% after regeneration at 700 °C; however, the rate of change in CH_4 conversion after each regeneration step was slower compared to the CH_4 conversion recovery after O_2 regeneration steps. No SO_2 desorption occurred during the regeneration steps at high temperatures or after the reintroduction of CH_4 oxidation conditions as shown in Fig. S6B. Alternating between periods of high H_2 concentrations and the presence of CH_4 and O_2 does not appear to induce the decomposition of S species into SO_2.

Alternating the feed composition between reductant- and oxygen-rich phases has been shown to be an effective regeneration method at low temperatures (< 600 °C) [68,69]. To test how alternating the feed composition affects regeneration, the CH_4 oxidation conditions (CH_4 – 1500 ppm + [O_2] – 0/5500 ppm + frequency = 0.25 Hz) were kept during temperature steps at 650 and 700 °C (Fig. S6A). After both temperature steps, CH_4 conversion improved to 90% verifying that feed fluctuations between the two phases did improve regeneration and catalyst performance. In evaluating the SO_2 profile during this regeneration protocol (Fig. S7B), only a small SO_2 desorption peak during the first regeneration ramp phase was observed. According to the literature, alternating the feed composition from reducing to oxidizing conditions leads to SO_2 release due to the reduction of stable sulfate species by CH_4 at the precious metal sites [68]. Even though SO_2 release during this regeneration was minimal, S species decomposition via the desorption of other S-containing species (i.e., H_2S) may have occurred.

Amplitude and frequency are key parameters during periodic operation that affect CH_4 oxidation performance [38–40], and these parameters can also potentially have an impact on the rate of S species decomposition on the PGM + spinel sample. First, the frequency of the [O_2] – 0/5500 ppm cycles was slowed from 0.25 to 0.0625 Hz. Fig. S8A shows the CH_4 conversion after regeneration at 700 °C, and it improved from 73% to 89% at 600 °C. In evaluating the S profile (Fig. S8B), some S desorbed from the catalyst surface in the presence of the regeneration gas conditions at 700 °C. Alternating the feed composition between the O-containing phase and its absence does lead to S release due to the reduction of sulfate species by CH_4 (or derived reductant). The faster frequency, 0.25 Hz, did not induce as much SO_2 release as shown in Fig. S7B. Slowing down the frequency to 0.0625 Hz may induce deeper reduction and/or also allow S species diffusion from the support to the precious metal sites which leads to more S species decomposition. Fig. 9 shows a summary of the CH_4 conversions after the application of these different regeneration methods, where key regeneration parameters, such as the regeneration temperature and the application of cycling, were introduced using the protocol described by Schematic S1.

Alternating the feed composition and optimizing cycling parameters during the regeneration process led to an increase in CH_4 conversion at 600 °C. The regeneration methods using cycling of the inlet gases discussed above include CH_4 as the reductant. Increasing the reductant concentration could lead to more S species decomposition during the regeneration step, which could in turn lead to an increase in catalyst performance. Fig. 10 A shows the CH_4 conversion and SO_2 profile before and after regeneration in a gas mixture that included H_2. The gas mixture was again modulated, with the O_2 cycling between 0/5500 ppm at a frequency of 0.0625 Hz, all at 700 °C. Note, the slower cycling frequency leads to more significant oscillations in the conversion as a function of time, especially at the higher temperature where deeper reduction can occur in the absence of O_2. With the addition of 0.1% H_2 to the regeneration feed composition, CH_4 conversion improved from 73% to 93%. Table 3 shows the S balance during adsorption and desorption during the CH_4 oxidation temperature ramp. This regeneration method with H_2 included was able to induce the decomposition of 87% of the adsorbed S species, which led to the catalytic activity recovery at 600 °C. Fig. 10B shows the comparison of the $O_{consumed}$ for fresh, SO_2-exposed, and regenerated Mn-Fe spinel powder using this regeneration protocol, and it successfully recovered all the $O_{consumed}$ lost after S exposure.

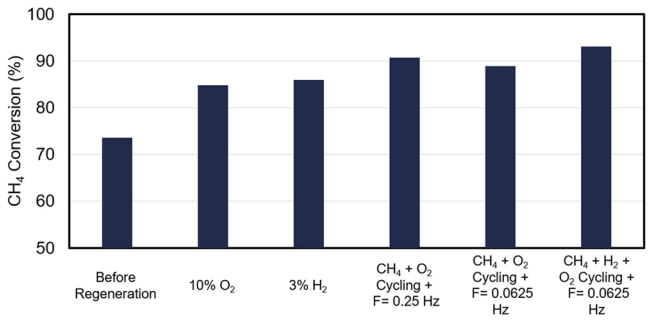

Fig. 9. Summary of CH_4 conversion after regeneration at 700 °C using Schematic S1.

To evaluate any effects due to the high temperature treatment, i.e., separate from that of S exposure combined with the high temperature treatment, a separate experiment was run duplicating all regeneration conditions excluding the sulfur exposure at 100 °C. Fig. S9 shows that methane conversion dropped from 100% to 90% during the first isothermal hold at 600 °C, suggesting that high temperature deactivation likely occurred (i.e., sintering or changes in oxygen storage properties). These results suggest that deactivation due to exposure at 600 °C could have affected the results for CH_4 oxidation and $O_{consumed}$ during CO pulse measurements after regeneration; however, high temperature exposure is needed for catalyst regeneration from S exposure. After the application of the regeneration step at 700 °C to the control sample, CH_4 conversion reached 89% at the second isothermal hold at 600 °C, showing that these regeneration conditions do not cause any further deactivation to the PGM + spinel sample. Comparing these control results with the high temperature regeneration results shown in Fig. 10 A, the combination of alternating the feed composition and optimizing cycling parameters regenerated the catalyst fully; however, thermal degradation did occur.

While some amount of CH_4 oxidation activity was recovered for all regeneration methods tested, the extent of regeneration depends on the ability to induce and drive the decomposition of SO_4^{-2} species, which influence the CH_4 oxidation performance at high temperatures on the PGM + spinel catalyst. Even though CH_4 conversion improved, regeneration methods with a constant feed composition (i.e., O_2 and H_2 conditions) did not induce the decomposition of all SO_4^{-2} species since no S release occurred during the regeneration steps as shown in Figs. S5B and S6B. It is likely these conditions do not drive S species decomposition since a highly oxidized or reduced S species cannot be released as SO_2. Once a reductant (i.e., CH_4) is reintroduced into the feed after O_2 regeneration steps as shown in Fig. S5B, the sulfate species can be reduced and S released as SO_2. In the case of H_2 regeneration, the small oxygen concentration during methane oxidation conditions might not be sufficient to drive SO_2 release from the highly reduced S species, or S was released during the regeneration step, but as H_2S which was not able to be measured. The latter is likely given the recovery of some CH_4 oxidation activity. Alternating the feed composition from reducing to oxidizing conditions results in more sulfate decomposition via the release of SO_2, since it avoids the formation of highly oxidized or reduced S species. With this in mind, the effects of cycling parameters (i.e., frequency) should and do lead to differences in the released S profiles as shown in Figs. S7B and S8B. Slower frequencies show a greater S release during the regeneration steps compared to the S release profile of the faster frequencies tested, suggesting that alternating the feed composition drives S diffusion on the catalyst surface. Ultimately, the decomposition of SO_4^{-2} species on the PGM + spinel catalyst is best achieved by the application of periodic operation in the presence of both reducing and oxidizing agents.

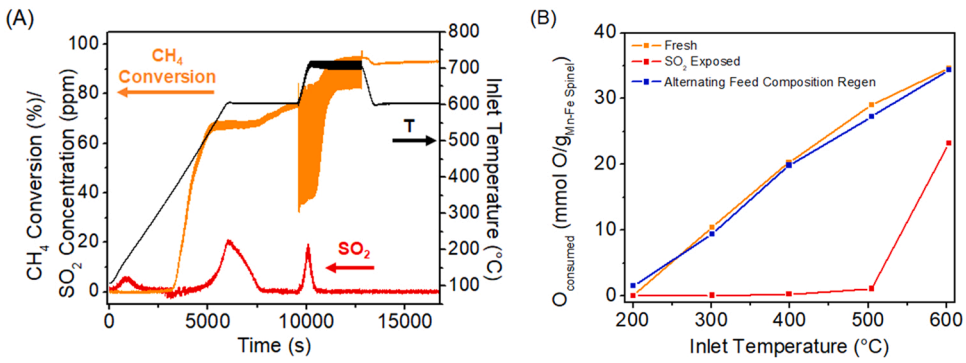

Fig. 10. (A) CH_4 conversion and SO_2 profile after regeneration at 700 °C with $CH_4 + H_2$ and cycling O_2 at a frequency = 0.0625 Hz step using the PGM + spinel monolith sample; (B) Comparison of the $O_{consumed}$ for the fresh, SO_2 exposed and regenerated (700 °C, $CH_4 + H_2 + [O_2]$ – 0/5500 ppm + frequency = 0.0625 Hz) Spinel Only powder. After SO_2 exposure at 100 °C, the CH_4 oxidation recovery was assessed using Schematic S1, and the $O_{consumed}$ was evaluated after exposure to regeneration conditions at 700 °C.

4. Conclusions

The effects of SO_2 exposure and subsequent catalyst regeneration on the methane oxidation performance of a bilayer PGM + $Mn_{0.5}Fe_{2.5}O_4$ spinel catalyst operating under periodic inlet gas composition conditions were studied. Improvement in CH_4 conversion under periodic conditions relative to steady-state inlet gas composition conditions was observed. A measure of the reactive oxygen associated with the $Mn_{0.5}Fe_{2.5}O_4$ spinel was probed via CO pulse injection and showed that oxygen from its spinel lattice can be released and be an oxygen source during the oxygen-deficient phases during periodic conditions. After sulfur exposure at 100 °C, the CH_4 oxidation performance loss over the PGM + spinel catalyst was due to the influence of SO_4^{-2} on the catalyst, and the loss of reactive O of the spinel material. The extent of regeneration of the PGM + spinel catalyst is dependent on the ability to induce the decomposition of the more stable SO_4^{-2} species, and while all regeneration methods tested in this study do improve CH_4 conversion at 600 °C, regeneration methods under periodic conditions not only improved CH_4 conversion, but also induced greater S species decomposition from the catalyst surface.

CRediT authorship contribution statement

Natalia Diaz Montenegro: Conceptualization, Methodology, Validation, Formal analysis, Investigation, Data curation, Writing – original draft, Visualization. **William Epling**: Conceptualization, Methodology, Formal analysis, Writing – review & editing, Visualization, Project administration, Funding acquisition.

Declaration of Competing Interest

The authors declare the following financial interests/personal relationships which may be considered as potential competing interests: William Epling reports financial support was provided by US Department of Energy. William Epling reports equipment, drugs, or supplies was provided by CDTi Advanced Materials, Inc.

Data availability

Data will be made available on request.

Acknowledgements

The authors gratefully acknowledge CDTi for the samples provided. The authors also acknowledge funding support from the United States Department of Energy under contract DOE-EE0008332.

Appendix A. Supporting information

Supplementary data associated with this article can be found in the online version at doi:10.1016/j.apcatb.2023.122894.

References

[1] R.A. Kerr, Natural gas from shale bursts onto the scene, Sci. Mag. vol. 328 (June) (2010) 1624–1626.
[2] S. Pischinger, M. Umierski, B. Hüchtebrock, New CNG concepts for passenger cars: high torque engines with superior fuel consumption, SAE Tech. Pap. Ser. vol. 1 (724) (2003), https://doi.org/10.4271/2003-01-2264.
[3] B.A. Raj, Methane emission control, Johns. Matthey Technol. Rev. vol. 60 (4) (. 2016) 228–235, https://doi.org/10.1595/205651316×692554.
[4] Intergovernmental Panel on Climate Change, Anthropogenic and Natural Radiative Forcing, vol. 6, Cambridge University Press,, Cambridge, 2014.
[5] F. Register, Greenh. Gas. Emiss. Fuel Effic. Stand. Medium- Heavy-Duty Engines Vehicles— Phase 2 vol. 81 (206) (2016) 73478–74274.
[6] R. Horn, R. Schlögl, Methane activation by heterogeneous catalysis, Catal. Lett. vol. 145 (1) (2015) 23–39, https://doi.org/10.1007/s10562-014-1417-z.
[7] E.D. German, M. Sheintuch, Predicting CH_4 dissociation kinetics on metals: Trends, sticking coefficients, H tunneling, and kinetic isotope effect, J. Phys. Chem. C. vol. 117 (44) (2013) 22811–22826, https://doi.org/10.1021/jp406937r.
[8] D. Jiang, K. Khivantsev, Y. Wang, Low-Temperature Methane Oxidaiton for Efficient Emission Control in Natural Gas Vehicles: Pd and beyond, ACS Catal. 10 (23) (. 2020) 14304–14314, https://doi.org/10.1021/acscatal.0c03338.
[9] P. Gélin, M. Primet, Complete oxidation of methane at low temperature over noble metal based catalysts: A review, Appl. Catal. B Environ. vol. 39 (1) (2002) 1–37, https://doi.org/10.1016/S0926-3373(02)00076-0.
[10] J. Wang, H. Chen, Z. Hu, M. Yao, Y. Li, A review on the Pd-based three-way catalyst, Catal. Rev. - Sci. Eng. vol. 57 (1) (2015) 79–144, https://doi.org/10.1080/01614940.2014.977059.
[11] R. Di Monte, J. Kašpar, On the role of oxygen storage in three-way catalysis, Top. Catal. vol. 28 (1–4) (2004) 47–58, https://doi.org/10.1023/B:TOCA.0000024333.08447.f7.
[12] E. Aneggi, M. Boaro, S. Colussi, C. de Leitenburg, and A. Trovarelli, Ceria-Based Materials in Catalysis: Historical Perspective and Future Trends, 1st ed., vol. 50. Elsevier B.V., 2016. doi: 10.1016/bs.hpcre.2016.05.002.
[13] R. Neha, Prasad, S.Vir Singh, Catalytic abatement of CO, HCs and soot emissions over spinel-based catalysts from diesel engines: An overview, J. Environ. Chem. Eng. vol. 8 (2) (2020), 103627, https://doi.org/10.1016/j.jece.2019.103627.
[14] S. Yang, C. Wang, J. Li, N. Yan, L. Ma, H. Chang, Low temperature selective catalytic reduction of NO with NH_3 over Mn-Fe spinel: Performance, mechanism and kinetic study, Appl. Catal. B Environ. vol. 110 (2011) 71–80, https://doi.org/10.1016/j.apcatb.2011.08.027.
[15] S.A. Hosseini, D. Salari, A. Niaei, F. Deganello, G. Pantaleo, P. Hojati, Chemical-physical properties of spinel $CoMn_2O_4$ nano-powders and catalytic activity in the 2-propanol and toluene combustion: Effect of the preparation method, J. Environ. Sci. Heal. - Part A Toxic. /Hazard. Subst. Environ. Eng. vol. 46 (3) (2011) 291–297, https://doi.org/10.1080/10934529.2011.539093.
[16] M. Zawadzki, W. Walerczyk, F.E. López-Suárez, M.J. Illán-Gómez, A. Bueno-López, $CoAl_2O_4$ spinel catalyst for soot combustion with NOx/O_2, Catal. Commun. vol. 12 (13) (2011) 1238–1241, https://doi.org/10.1016/j.catcom.2011.04.021.
[17] H. Lin, Y. Li, W. Shangguan, Z. Huang, Soot oxidation and NOx reduction over $BaAl_2O_4$ catalyst, Combust. Flame vol. 156 (11) (2009) 2063–2070, https://doi.org/10.1016/j.combustflame.2009.08.006.
[18] S.O. Soloviev, A.Y. Kapran, Y.P. Kurylets, Oxidation of diesel soot on binary oxide CuCr(Co)-based monoliths, J. Environ. Sci. (China) vol. 28 (2015) 171–177, https://doi.org/10.1016/j.jes.2014.08.017.
[19] D. Fino, N. Russo, G. Saracco, V. Specchia, Removal of NOx and diesel soot over catalytic traps based on spinel-type oxides, Powder Technol. vol. 180 (1–2) (2008) 74–78, https://doi.org/10.1016/j.powtec.2007.03.003.
[20] W.F. Shangguan, Y. Teraoka, and S. Kagawa, Simultaneous catalytic removal of NO, and diesel soot particulates over ternary AB_2O_4 spinel-type oxides, 1996.
[21] P. Mountapmbeme Kouotou, H. Vieker, Z.Y. Tian, P.H. Tchoua Ngamou, A. El Kasmi, A. Beyer, A. Golzhauser, K. Hohse-Hoinghaus, Structure-activity relation of spinel-type Co-Fe oxides for low-temperature CO oxidation, Catal. Sci. Technol. vol. 4 (9) (2014) 3359–3367, https://doi.org/10.1039/c4cy00463a.

[22] S. Trivedi, R. Prasad, S.K. Gautam, Design of active $NiCo_2O_{4-\delta}$ spinel catalyst for abatement of CO-CH_4 emissions from CNG fueled vehicles, AIChE J. vol. 64 (7) (2018) 2632–2646, https://doi.org/10.1002/aic.16162.

[23] J. Li, X. Liang, S. Xu, J. Hao, Catalytic performance of manganese cobalt oxides on methane combustion at low temperature, Appl. Catal. B Environ. vol. 90 (1–2) (2009) 307–312, https://doi.org/10.1016/j.apcatb.2009.03.027.

[24] S. Golden, Z. Nazarpoor, M. Launois, Novel mixed metal oxide structure for next generation three-way catalysts, SAE Int. vol. 2015–01–10 (2015), https://doi.org/10.4271/2015-01-1007.

[25] Z. Nazarpoor and S.J. Golden, Thermally Stable Compositions of OSM Free of Rare Earth Metals, 9.486,784 B2, 2016.

[26] S. Golden, Z. Nazarpoor, R.-F. Liu, TWC Using Advanced Spinel Materials and Prospects for BSVI Compliance, SAE Int. vol. 2017–26–01 (2017), https://doi.org/10.4271/2017-26-0126.Copyright.

[27] S. Golden, Z. Nazarpoor, M. Launois, R.F. Liu, P. Maram, Development of Non-Copper Advanced Spinel Mixed Metal Oxides for Zero-Precious Metal and Ultra-Low Precious Metal Next-Generation TWC, in, *SAE Tech. Pap.*, SAE Int. (2016), https://doi.org/10.4271/2016-01-0933.

[28] S.B. Kang, K. Karinshak, P.W. Chen, S. Golden, M.P. Harold, Coupled methane and NOx conversion on Pt + Pd/Al_2O_3 monolith: Conversion enhancement through feed modulation and Mn0.5Fe2.5O4 spinel addition, Catal. Today vol. 360 (2021) 284–293, https://doi.org/10.1016/j.cattod.2020.02.039.

[29] S. Fouladvand, M. Skoglundh, P.A. Carlsson, A transient in situ infrared spectroscopy study on methane oxidation over supported Pt catalysts, Catal. Sci. Technol. vol. 4 (10) (2014) 3463–3473, https://doi.org/10.1039/c4cy00486h.

[30] P.A. Carlsson, E. Fridell, M. Skoglundh, Methane oxidation over Pt/Al_2O_3 and Pd/Al_2O_3 catalysts under transient conditions, Catal. Lett. vol. 115 (1–2) (2007) 1–7, https://doi.org/10.1007/s10562-007-9057-1.

[31] D. Bounechada, G. Groppi, P. Forzatti, K. Kallinen, T. Kinnunen, Effect of periodic lean/rich switch on methane conversion over a Ce-Zr promoted $Pd-Rh/Al_2O_3$ catalyst in the exhausts of natural gas vehicles, Appl. Catal. B Environ. vol. 119–120 (2012) 91–99, https://doi.org/10.1016/j.apcatb.2012.02.025.

[32] S. Fouladvand, M. Skoglundh, P.A. Carlsson, Unsteady-state operation of supported platinum catalysts for high conversion of methane, Chem. Eng. J. vol. 292 (2016) 321–325, https://doi.org/10.1016/j.cej.2016.02.033.

[33] P.A. Carlsson, S. Mollner, K. Arnby, M. Skoglundh, Effect of periodic operation on the low-temperature activity for propane oxidation over Pt/Al_2O_3 catalysts, Chem. Eng. Sci. vol. 59 (20) (2004) 4313–4323, https://doi.org/10.1016/j.ces.2004.06.024.

[34] E. Becker, P.A. Carlsson, H. Grönbeck, M. Skoglundh, Methane oxidation over alumina supported platinum investigated by time-resolved in situ XANES spectroscopy, J. Catal. vol. 252 (1) (2007) 11–17, https://doi.org/10.1016/j.jcat.2007.09.004.

[35] E. Becker, P.A. Carlsson, L. Kylhammar, M.A. Newton, M. Skoglundh, In situ spectroscopic investigation of low-temperature oxidation of methane over alumina-supported platinum during periodic operation, J. Phys. Chem. C. vol. 115 (4) (2011) 944–951, https://doi.org/10.1021/jp103609n.

[36] Y.H. Chin, C. Buda, M. Neurock, E. Iglesia, Reactivity of Chemisorbed Oxygen Atoms and Their Catalytic Consequences during CH_4-O_2 Catalysis on Supported Pt Clusters, J. Am. Chem. Soc. vol. 133 (40) (2011) 15958–15978, https://doi.org/10.1021/ja202411v.

[37] Z. Zhou, M.P. Harold, D. Luss, Enhanced NO, CO and C_3H_6 conversion on Pt/Pd catalysts: Impact of oxygen storage material and catalyst architecture, Catal. Today (October 2019) (2020) 1–13, https://doi.org/10.1016/j.cattod.2020.01.026.

[38] K. Karinshak, P.W. Chen, R.-F. Liu, S.J. Golden, M.P. Harold, Optimizing feed modulation for coupled methane and NOx conversion over $Pd-Pt/Mn_{0.5}Fe_{2.5}O_4/Al_2O_3$ monolith catalyst, Appl. Catal. B Environ. vol. 304 (x) (2022), 120607, https://doi.org/10.1016/j.apcatb.2021.120607.

[39] J. Gong, J. Pihl, D. Wang, M.-Y. Kin, W.P. Partridge, J. Li, M. Cunningham, K. Kamasamudram, N. Currier, A. Yezerets, O_2 dosage as a descriptor of TWC performance under lean/rich dithering in stoichiometric natural gas engines, Catal. Today vol. 360 (February) (2021) 294–304, https://doi.org/10.1016/j.cattod.2020.02.022.

[40] M. Roger, O. Kröcher, D. Ferri, Assessing the effect of O_2 dithering on CH_4 oxidation on Pd/Al_2O_3, Chem. Eng. J. vol. 451 (4) (2023), 138865, https://doi.org/10.1016/j.cej.2022.138865.

[41] H.S. Gandhi, M. Shelef, Effects of sulphur on noble metal automotive catalysts, Appl. Catal. vol. 77 (2) (1991) 175–186, https://doi.org/10.1016/0166-9834(91)80063-3.

[42] J.K. Lampert, M.S. Kazi, R.J. Farrauto, Palladium catalyst performance for methane emissions abatement from lean burn natural gas vehicles, Appl. Catal. B Environ. vol. 14 (3–4) (1997) 211–223, https://doi.org/10.1016/S0926-3373(97)00024-6.

[43] H.N. Sharma, V. Sharma, A.B. Mhadeshwar, R. Ramprasad, Why Pt survives but Pd suffers from SOx poisoning? J. Phys. Chem. Lett. vol. 6 (7) (2015) 1140–1148, https://doi.org/10.1021/jz5027147.

[44] W. Yang, J. Gong, X. Wang, Z. Bao, Y. Guo, Z. Wu, A Review on the Impact of SO_2 on the Oxidation of NO, Hydrocarbons, and CO in Diesel Emission Control Catalysis, in: ACS Catalysis, vol. 11, American Chemical Society,, 2021, pp. 12446–12468, https://doi.org/10.1021/acscatal.1c03013.

[45] D.L. Mowery, R.L. McCormick, Deactivation of alumina supported and unsupported PdO methane oxidation catalyst: The effect of water on sulfate poisoning, Appl. Catal. B Environ. vol. 34 (4) (2001) 287–297, https://doi.org/10.1016/S0926-3373(01)00222-3.

[46] P. Auvinen, J.T. Hirvi, N.M. Kinnunen, M. Suvanto, $PdSO_4$ Surfaces in Methane Oxidation Catalysts: DFT Studies on Stability, Reactivity, and Water Inhibition, ACS Catal. vol. 10 (21) (2020) 12943–12953, https://doi.org/10.1021/acscatal.0c03686.

[47] M.Y. Smirnov, A.V. Kalinkin, A.V. Pashis, I.P. Prosvirin, V.I. Bukhtiyarov, Interaction of SO_2 with Pt model supported catalysts studied by XPS, J. Phys. Chem. C. vol. 118 (38) (2014) 22120–22135, https://doi.org/10.1021/jp5069126.

[48] R.M. Ferrizz, R.J. Gorte, J.M. Vohs, TPD and XPS investigation of the interaction of SO_2 with model ceria catalysts, Catal. Lett. vol. 82 (1–2) (2002) 123–129, https://doi.org/10.1023/A:1020512713021.

[49] C.C. Chang, Infrared studies of SO_2 on γ-alumina, J. Catal. vol. 53 (3) (1978) 374–385, https://doi.org/10.1016/0021-9517(78)90109-4.

[50] M.Y. Smirnov, A.V. Kalinkin, A.V. Pashis, A.M. Sorokin, A.S. Noskov, K.C. Kharas, V.I. Bukhtiyarov, Interaction of Al_2O_3 and CeO_2 Surfaces with SO_2 and SO_2 + O_2 studied by X-ray Photoelectron Spectroscopy, J. Phys. Chem. B vol. 109 (23) (2005) 11712–11719, https://doi.org/10.1021/jp0508249.

[51] L.S. Escandón, S. Ordóñez, A. Vega, F.V. Díez, Sulphur poisoning of palladium catalysts used for methane combustion: Effect of the support, J. Hazard. Mater. vol. 153 (1–2) (2008) 742–750, https://doi.org/10.1016/j.jhazmat.2007.09.017.

[52] M.S. Wilburn, W.S. Epling, SO_2 adsorption and desorption characteristics of Pd and Pt catalysts: Precious metal crystallite size dependence, Appl. Catal. A Gen. vol. 534 (2017) 85–93, https://doi.org/10.1016/j.apcata.2017.01.015.

[53] M.S. Wilburn, W.S. Epling, Sulfur deactivation and regeneration of mono- and bimetallic Pd-Pt methane oxidation catalysts, Appl. Catal. B Environ. vol. 206 (2017) 589–598, https://doi.org/10.1016/j.apcatb.2017.01.050.

[54] M.S. Wilburn and W.S. Epling, A Summary of Sulfur Deactivation, Desorption, and Regeneration Characteristics of Mono- and Bimetallic Pd-Pt Methane Oxidation Catalysts: Pd:Pt Mole Ratio and Particle Size Dependency, pp. 78–89, 2018.

[55] G. Corro, C. Cano, J.L.G. Fierro, A study of $Pt-Pd/\gamma-Al_2O_3$ catalysts for methane oxidation resistant to deactivation by sulfur poisoning, J. Mol. Catal. A Chem. vol. 315 (1) (2010) 35–42, https://doi.org/10.1016/j.molcata.2009.08.023.

[56] N. Sadokhina, G. Smedler, U. Nylén, M. Olofsson, L. Olsson, Deceleration of SO_2 poisoning on $PtPd/Al_2O_3$ catalyst during complete methane oxidation, Appl. Catal. B Environ. vol. 236 (May) (2018) 384–395, https://doi.org/10.1016/j.apcatb.2018.05.018.

[57] P. Lott, M. Eck, D.E. Doronkin, A. Zimina, S. Tischer, R. Popescu, S. Belin, V. Briois, M. Capasu, J.-D. Grunwaldt, O. Deutschmann, Understanding sulfur poisoning of bimetallic Pd-Pt methane oxidation catalysts and their regeneration, Appl. Catal. B Environ. vol. 278 (April) (2020), 119244, https://doi.org/10.1016/j.apcatb.2020.119244.

[58] M. Tepluchin, S. Kureti, M. Casapu, E. Ogel, S. Mangold, J.D. Grunwaldt, Study on the hydrothermal and SO_2 stability of Al_2O_3-supported manganese and iron oxide catalysts for lean CO oxidation, Catal. Today vol. 258 (2015) 498–506, https://doi.org/10.1016/j.cattod.2015.01.010.

[59] F. Lin, Y. He, Z. Wang, Q. Ma, R. Whiddon, Y. Zhu, J. Lie, Catalytic oxidation of NO by O_2 over CeO_2-MnO_x: SO_2 poisoning mechanism, RSC Adv. vol. 6 (37) (2016) 31422–31430, https://doi.org/10.1039/c6ra03818b.

[60] Y. Zhang, P. Glarborg, M.P. Andersson, K. Johansen, T.K. Torp, A.D. Jensen, Sulfur poisoning and regeneration of Rh-ZSM-5 catalysts for total oxidation of methane, Appl. Catal. B Environ. vol. 277 (2020), https://doi.org/10.1016/j.apcatb.2020.119176.

[61] J.Y. Luo, D. Kisinger, A. Abedi, W.S. Epling, Sulfur release from a model Pt/Al_2O_3 diesel oxidation catalyst: Temperature-programmed and step-response techniques characterization, Appl. Catal. A Gen. vol. 383 (1–2) (2010) 182–191, https://doi.org/10.1016/j.apcata.2010.05.049.

[62] P. Bazin, O. Saur, O. Marie, M. Daturi, J.C. Lavalley, A.M. Le Govic, V. Harle, G. Blanchard, On the reducibility of sulfated $Pt/Ce_XZr_{1-X}O_2$ solids: A coupled thermogravimetric FT-IR study using CO as the reducing agent, Appl. Catal. B Environ. vol. 119–120 (2012) 207–216, https://doi.org/10.1016/j.apcatb.2012.02.037.

[63] T. Luo, R.J. Gorte, Characterization of SO_2-poisoned ceria-zirconia mixed oxides, Appl. Catal. B Environ. vol. 53 (2) (2004) 77–85, https://doi.org/10.1016/j.apcatb.2004.04.020.

[64] V.H. Nissinen, N.M. Kinnunen, M. Suvanto, Regeneration of a sulfur-poisoned methane combustion catalyst: Structural evidence of Pd_4S formation, Appl. Catal. B Environ. vol. 237 (2018) 110–115, https://doi.org/10.1016/j.apcatb.2018.05.057.

[65] F. Cabello Galisteo, R. Mariscal, M. Lopez Granados, M.D. Zafra Poves, J.L. G. Fierro, V. Kroger, R.L. Keiski, Reactivation of sulphated Pt/Al_2O_3 catalysts by reductive treatment in the simultaneous oxidation of CO and C_3H_6, Appl. Catal. B Environ. vol. 72 (3–4) (2007) 272–281, https://doi.org/10.1016/j.apcatb.2006.11.004.

[66] P. Bazin, O. Saur, F. Meunier, M. Daturi, J.C. Lavalley, A.M. Le Govic, V. Harle, G. Blanchard, A thermogravimetric and FT-IR study of the reduction by H_2 of sulfated $Pt/Ce_xZr_{1-x}O_2$ solids, Appl. Catal. B Environ. vol. 90 (3–4) (2009) 368–379, https://doi.org/10.1016/j.apcatb.2009.03.016.

[67] N. Ottinger, R. Veele, Y. Xi, Z.G. Liu, Desulfation of Pd-based Oxidation Catalysts for Lean-burn Natural Gas and Dual-fuel Applications, SAE Int. J. Engines vol. 8 (4) (2015) 1472–1477, https://doi.org/10.4271/2015-01-0991.

[68] F. Arosio, S. Colussi, A. Trovarelli, G. Groppi, Effect of alternate CH_4-reducing/lean combustion treatments on the reactivity of fresh and S-poisoned $Pd/CeO_2/Al_2O_3$ catalysts, Appl. Catal. B Environ. vol. 80 (3–4) (2008) 335–342, https://doi.org/10.1016/j.apcatb.2007.11.030.

[69] F. Arosio, S. Colussi, G. Groppi, A. Trovarelli, Regeneration of S-poisoned Pd/Al_2O_3 catalysts for the combustion of methane, Catal. Today vol. 117 (4) (2006) 569–576, https://doi.org/10.1016/j.cattod.2006.06.006.

[70] N.M. Kinnunen, V.H. Nissinen, J.T. Hirvi, K. Kallinen, T. Mainula, M. Keenan, M. Suvanto, Decomposition of Al_2O_3-supported $PdSO_4$ and $Al_2(SO_4)_3$ in the

regeneration of methane combustion catalyst: A model catalyst study, Catalysts vol. 9 (5) (2019), https://doi.org/10.3390/catal9050427.
[71] S. Ordóñez, P. Hurtado, F.V. Díez, Methane catalytic combustion over Pd/Al_2O_3 in presence of sulphur dioxide: Development of a regeneration procedure, Catal. Lett. vol. 100 (1–2) (2005) 27–34, https://doi.org/10.1007/s10562-004-3081-1.
[72] A. Gremminger, P. Lott, M. Merts, M. Casapu, J.D. Grunwaldt, O. Deutschmann, Sulfur poisoning and regeneration of bimetallic Pd-Pt methane oxidation catalysts, Appl. Catal. B Environ. vol. 218 (2017) 833–843, https://doi.org/10.1016/j.apcatb.2017.06.048.
[73] J.M. Jones, V.A. Dupont, R. Brydson, D.J. Fullerton, N.S. Nasri, A.B. Ross, A.V. K. Westwood, Sulphur poisoning and regeneration of precious metal catalysed methane combustion, Catal. Today vol. 81 (4) (2003) 589–601, https://doi.org/10.1016/s0920-5861(03)00157-3.
[74] N.M. Kinnunen, J.T. Hirvi, K. Kallinen, T. Maunula, M. Keenan, M. Suvanto, Case study of a modern lean-burn methane combustion catalyst for automotive applications: What are the deactivation and regeneration mechanisms, Appl. Catal. B Environ. vol. 207 (2017) 114–119, https://doi.org/10.1016/j.apcatb.2017.02.018.
[75] P.W. Chen, D. Maiti, R.F. Liu, L.C. Grabow, M.P. Harold, CH_4 steam reforming on Pt + Pd/Al_2O_3 monolith: Impact of $Mn_{0.5}Fe_{2.5}O_4$ spinel addition, Catal. Sci. Technol. (2022) 2618–2633, https://doi.org/10.1039/d2cy00270a.
[76] Z. Zhou, M.P. Harold, D. Luss, Dynamic Oxygen Storage Capacity of Ceria-Zirconia and $Mn_{0.5}Fe_{2.5}O_4$ Spinel: Experiments and Modeling, Ind. Eng. Chem. Res. (2021), https://doi.org/10.1021/acs.iecr.0c05187.
[77] P.L. Silveston, Automotive exhaust catalysis under periodic operation, Catal. Today vol. 25 (2) (1995) 175–195, https://doi.org/10.1016/0920-5861(95)00107-Q.
[78] R. Burch, P.K. Loader, Investigation of Pt/Al_2O_3, and Pd/Al_2O_3 catalysts for the combustion of methane at low concentrations 5 (1994) 149–164.
[79] H.C. Yao, Y.F.Y. Yao, Ceria in automotive exhaust catalysts. I. Oxygen storage, J. Catal. vol. 86 (2) (1984) 254–265, https://doi.org/10.1016/0021-9517(84)90371-3.
[80] A. Hinz, A. Andersson, M. Skoglundh, E. Fridell, An investigation of the reaction mechanism for the promotion of propane oxidation over Pt/Al_2O_3 by SO_2, J. Catal. vol. 201 (2) (2001) 247–257, https://doi.org/10.1006/jcat.2001.3248.
[81] R. Burch, E. Halpin, M. Hayes, K. Ruth, J.A. Sullivan, The nature of activity enhancement for propane oxidation over supported Pt catalysts exposed to sulphur dioxide, Appl. Catal. B Environ. vol. 19 (3–4) (1998) 199–207, https://doi.org/10.1016/S0926-3373(98)00079-4.
[82] A.F. Lee, K. Wilson, R.M. Lambert, C.P. Hubbard, R.G. Hurley, R.W. McCabe, H. S. Gandhi, The origin of SO_2 promotion of propane oxidation over Pt/Al_2O_3 catalysts, J. Catal. vol. 184 (2) (1999) 491–498, https://doi.org/10.1006/jcat.1999.2454.
[83] D. Bounechada, S. Fouladvand, L. Kylhammar, T. Pingel, E. Olsson, M. Skoglundh, J. Gustafson, M. Di Michiel, M.A. Newton, P.-A. Carlsson, Mechanisms behind sulfur promoted oxidation of methane, Phys. Chem. Chem. Phys. vol. 15 (22) (2013) 8648–8661, https://doi.org/10.1039/c3cp44289f.
[84] A. Melchor, E. Garbowski, M.V. Mathieu, and M. Primet, Sulfur Poisoning of Pt/Al_2O_3 Catalysts, I. Determination of Sulfur Coverage by Infrared Spectroscopy, 1985.
[85] S. Hilaire, S. Sharma, R.J. Gorte, J.M. Vohs, H.W. Jen, Effect of SO_2 on the oxygen storage capacity of ceria-based catalysts, Catal. Lett. vol. 70 (3–4) (2000) 131–135, https://doi.org/10.1023/A:1018885201072.
[86] O. Saur, M. Bensitel, A.B.M. Saad, J.C. Lavalley, C.P. Tripp, B.A. Morrow, The structure and stability of sulfated alumina and titania, J. Catal. vol. 99 (1) (1986) 104–110, https://doi.org/10.1016/0021-9517(86)90203-4.